Physics of the Earth and Planetary Interiors, 68 (1991) 9–31
Elsevier Science Publishers B.V., Amsterdam

Remelting mechanisms for shallow source regions of mare basalts

Michael Manga [1] and Jafar Arkani-Hamed

Department of Geological Sciences, McGill University, 3450 University Street, Montreal, Que. H3A 2A7, Canada

(Received 3 September 1990; revision accepted 7 March 1991)

ABSTRACT

Manga, M. and Arkani-Hamed, J., 1991. Remelting mechanisms for shallow source regions of mare basalts. Phys. Earth Planet. Inter., 68: 9–31.

Two mechanisms are studied which could induce remelting at shallow depths within the Moon: a radioactive heating model in which remelting is the result of lateral variations of the heat source concentration emplaced by the end of the initial differentiation event, and a thermal insulation model in which remelting is induced by lateral variations of near-surface conductivity as a result of a high-porosity ejecta blanket created by basin-forming impacts. The effects of these perturbations are studied by evaluating the thermal evolution of an otherwise radially symmetric lunar model. The radioactive heating models predict extensive pre-basin volcanism, which would probably remove from the source region many of the heat-producing elements potentially responsible for melting. Therefore, localized high concentrations of heat-producing elements emplaced early would most probably not be heat sources for the basin-filling mare basalts; however, they are plausible heat sources for pre-basin mare basalts. The thermal insulation model predicts a delay of about 200 m.y. between impact and volcanism. Thermal insulation may also allow for the persistence of source regions for young basalts at shallow depths. If greater basin ages are correct, from 4.2 to 3.9 Ga, and most volcanism occurred between 3.8 and 3.6 Ga, then the thermal insulation model may explain the delay between impact and basin filling. If the basins formed during a terminal cataclysmic event at about 3.9 Ga, then the earliest stages of basin filling at about 3.8 Ga may have been a result of melting beneath the basin as a result of mantle uplift. Basin filling may have been characterized by a migration of the source region from beneath the basin to beneath the adjacent highlands. Cooling of the top 200 km beneath the basin after 200 m.y. because of its high surface conductivity is consistent with the mascon support requirement.

1. Introduction

Lunar mare basalts cover 17% of the Moon's surface, filling low-lying regions and impact basins. They account for less than 1% of the mass of the crust (Head, 1976), yet their origins have important implications for the composition and thermal history of the Moon. The origin and petrogenesis of these basalts has been a widely disputed topic for the past 20 years, and no single model for their origin has been widely accepted. Early suggestions that the lunar maria are impact melts (Urey, 1952) or deep pools of dust (Gold, 1956) were rejected when it was realized that the maria are compositionally distinct from the highlands (e.g. Ringwood and Essene, 1970), and are several hundred million years younger than the basins (e.g. Baldwin, 1963). Mare basalts are thought to have been derived from the partial remelting of mantle source regions, although they may be due to the persistence of intercumulus liquids (Hubbard and Minear, 1975). Several remelting mechanisms have been proposed: viscous energy dissipation during rebound after impact (Hulme, 1974), pressure release by the rapid rebound of the lunar mantle after impact (Kunze, 1974), tidal energy dissipation (Wones and Shaw, 1975), magma assimilation and hybridization involving melt that

[1] Present address: Department of Earth and Planetary Sciences, Harvard University, 20 Oxford Street, Cambridge, MA 02138, USA.

0031-9201/91/$03.50

originated from an initially cold deep interior (Ringwood and Kesson, 1976; Turcotte and Ahern, 1978), melting in the upwellings of early convection in the deep interior (Chacko and De-Bremaeker, 1982), heating caused by local concentrations of heat-producing elements (Hollister, 1975; Taylor, 1978), and thermal insulation by ejecta blankets (Arkani-Hamed, 1973c, 1974).

Neither viscous dissipation (Hulme, 1974) nor pressure release induced melting (Kunze, 1974) is consistent with the extended duration of mare volcanism as most basin rebound occurs nearly instantaneously on geological time-scales. If tidal energy dissipation (Wones and Shaw, 1975) was to provide sufficient energy to melt the source regions, the Moon would have had to have been very close to the Earth; this may have been the case early in lunar history, but the Moon would have receded quickly if tidal dissipation was significant (Kaula, 1971). Models involving heat provided by early convection (Chacko and De-Bremaeker, 1982) or melt that originated from the deep interior (e.g. Ringwood and Kesson, 1976; Turcotte and Ahern, 1978) apply only to a Moon with an initially cold interior; in these models the undifferentiated deep interior warms up by radioactive heating and convection is initiated, or melt is removed upwards by diapirism or melt migration. A Moon formed after the impact of a Mars-sized body with the Earth (Stevenson, 1987) or by binary fission (Binder and Lange, 1980) would probably be initially totally molten. Evidence that the entire Moon was initially totally molten comes from the magnitude of shallow moonquakes (Binder and Oberst, 1985) and the presence of 10 km-scale thrust faults (Binder and Gunga, 1985), consistent with estimated compressional stresses caused by significant thermal contraction, and a possible paleomagnetic requirement of an early iron core to account for the observed surface magnetization (Runcorn, 1977). However, the presence of volatile-rich regions in the Moon inferred from very large Ge enrichments in aluminous mare basalts and KREEP suggest that the Moon was never totally molten (Dickinson et al., 1989). An initially totally molten Moon would have been largely differentiated, leaving only small amounts of heat-producing elements and other incompatible elements in the deep interior, making the deep interior an unlikely ultimate source region for mare basalts.

Because of the uncertainty of the early thermal state of the Moon, mechanisms which could induce remelting at shallow depths, within the top 400 km, will be studied. Two remelting models are considered: a radioactive heating model in which heterogeneities in the concentration of heat-producing elements are emplaced by the end of the initial differentiation event, and a thermal insulation model in which lateral variations of near-surface thermal conductivity, a result of a high-porosity ejecta blanket, are created by basin-forming impacts. Both models apply to either a Moon with an initially cold interior covered by a magma ocean or to an initially totally molten Moon. These two models are studied by looking at the thermal evolution of an otherwise radially symmetric Moon. The feasibility of each model can be evaluated with respect to constraints imposed by observations of lunar volcanism in space and time.

2. Models

2.1. Radially symmetric model

The two models studied, radioactive heating and thermal insulation, involve the perturbation of a radially symmetric Moon. Therefore, a symmetric Moon is considered first in detail to obtain a plausible model to be later disturbed by either heterogeneities of heat sources or lateral variations of thermal conductivity. The initial conditions for the radially symmetric model, at time 4.4 Ga, after an initial differentiation event, are based on the cumulate source model in which the molten part of the Moon differentiated quickly by fractional crystallization to produce a plagioclase-rich crust and a compositionally stratified Moon (Taylor and Jakes, 1974). The initial temperature, immediately after the solidification of the magma ocean, follows a peridotite solidus to the base of the crust at 60 km, and decreases linearly to 0 °C at the surface (Fig. 1a). This initial condition is similar to those used for the initially molten part

of the Moon by other investigators (e.g. Toksöz et al., 1978; Binder and Lange, 1980). The liquidus and solidus used are those for a dry peridotite (Millhollen et al., 1974). As the molten part of the Moon solidifies, there is an upward concentration of incompatible elements towards the base of the crust, producing the KREEP layer, rich in REE and incompatible elements. The radially symmetric distribution of heat-producing elements has a maximum concentration in this layer, at depths from 60 to 80 km; the concentration decreases exponentially with depth, with a skin depth of 60 km (Fig. 1b), identical to that used by Hubbard and Minear (1975), i.e. the relative abundance of heat-producing elements decreases by a factor of $1/e$ of its value every 60 km. This skin depth was chosen so that basalts originating at a depth of 150 km from a region of 15% melt would have a concentration of uranium approximately equal to the average concentration in mare basalts, 240 ppb (Brown, 1977). For the calculations presented here the Moon was assumed to have been initially totally molten; this assumption affects only the distribution of heat-producing elements. Assuming instead the differentiation of a magma ocean 500 km deep would reduce the concentration of heat-producing elements by 36%; the thermal evolution of a model assuming whole-Moon differentiation and 20 ppb uranium is approximately equivalent to a model with a 500 km deep magma ocean and 27 ppb uranium.

Heat generation is provided by the long-lived isotopes ^{238}U, ^{235}U, ^{232}Th, and ^{40}K. The present-day bulk uranium abundance is assumed to be 20 ppb. This value is lower than an initial estimate of 60 ppb (Toksöz and Solomon, 1973) and a revised estimate of 46 ppb (Langseth et al., 1976) based on two heat flow measurements, because these

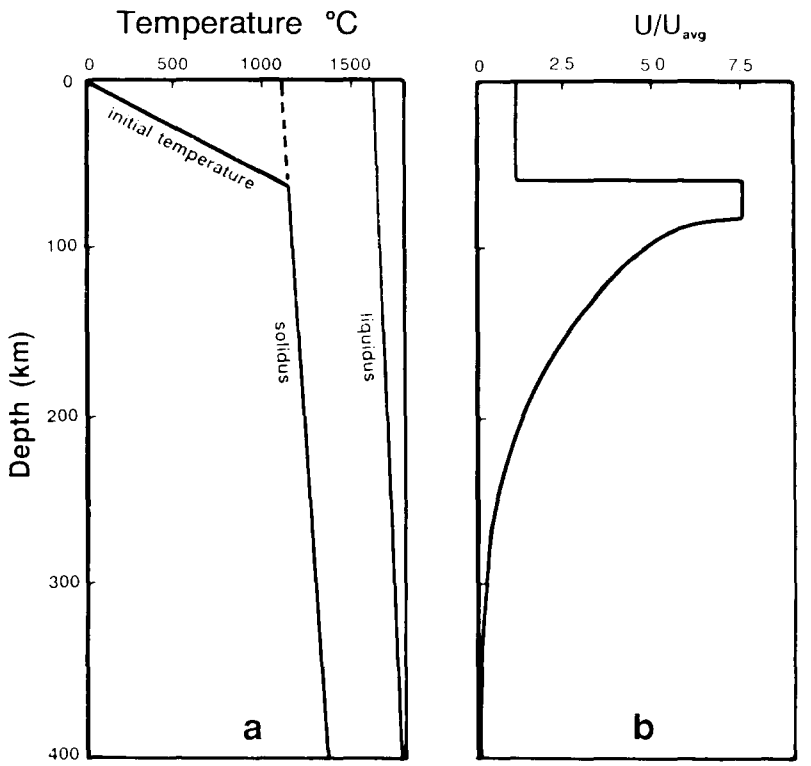

Fig. 1. (a) Initial temperature distribution at 4.4 Ga. The solidus and liquidus are for dry peridotite (Millhollen et al., 1974). (b) Normalized heat-producing element distribution based on Taylor and Jakes (1974), with a maximum at depths from 60 to 80 km, and decaying exponentially with depth with a skin depth of 60 km. Whole-Moon differentiation is assumed.

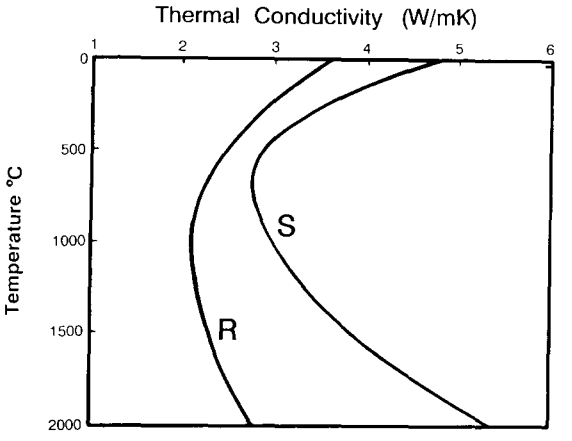

Fig. 2. Thermal conductivity model used in this paper. Conductivity is for olivine (Roy et al., 1981) modified to account for radiation effects at high temperatures (curve R). Also shown is the conductivity model of Schatz and Simmons (1972) (curve S).

estimates neglected the effects of global cooling (Schubert et al., 1980) and heat flow focusing at mare edges (Conel and Morton, 1975; Warren and Rasmussen, 1987). The value of 20 ppb is equal to estimates of the bulk uranium abundance in the Earth's crust and upper mantle (Ringwood, 1979) and only 3 ppb larger than the most recent estimate for the Moon (Warren and Rasmussen, 1987).

The temperature-dependent thermal conductivity model used in this paper is the mean conductivity for olivine (Roy et al., 1981) to which an estimate of the contribution of radiation at higher temperatures has been added (Fig. 2). Thermal conductivity, K, depends more strongly on porosity than composition—the conductivity of anorthite is about one-half the conductivity of pyroxene and olivine (Horai, 1971) whereas the high-porosity lunar soils have conductivities more than two orders of magnitude smaller (Langseth et al., 1976). Although the measured conductivity of lunar rocks correlates strongly with their porosity (Fig. 1, Warren and Rasmussen, 1987) the nature of the porosity is more important than the degree of porosity; microcracks, i.e. pores with a high aspect ratio, have a very significant effect on conductivity but contribute little to porosity (Francl and Kingery, 1954; Walsh and Decker, 1966). The effect of vacuum conditions further reduces the conductivity of porous rocks, but the difference between atmospheric and vacuum conditions decreases as temperature increases because of radiative effects (Fujii and Osako, 1973); conductivity was found to decrease with pressure until 10^{-3} Torr (Bernett et al., 1963; Mitzutani and Osako, 1974). Thus, it is expected that the highly fractured breccias in the megaregolith, a layer of high-porosity, impact-fractured rocks, would have a significantly reduced conductivity and, hence, it would act as a thermal blanket. Highland rock 77017 with $K = 0.2$ W mK^{-1} (Horai and Winkler, 1976) is thought to be representative of highland breccias, although it appears to be more highly sintered than most breccias (Warren and Rasmussen, 1987). This is the thermal conductivity assumed for the megaregolith in this study, although the actual conductivity may differ by as much as a factor of two (Warren and Rasmussen, 1987).

The radially symmetric Moon is assumed to be covered by a uniform thickness megaregolith. The megaregolith, assumed to be 1 km thick, based on seismic studies (Warren and Trice, 1977), is underlain by a fractured zone extending to the seismic discontinuity at 20 km (Toksöz et al., 1974). A megaregolith 1 km thick, thinner than other estimates of 2–4 km (e.g. Golombek and McGill, 1983), is chosen to be representative of the radially symmetric, unperturbed Moon. The present-day thickness includes ejecta and fracturing caused by the basin-forming impacts, effects which are not included in the radially symmetric Moon model and the radioactive heating model, only in the thermal insulation model. The conductivity of the upper 20 km is assumed to be 1.5 W mK^{-1}, in accordance with Keihm and Langseth (1977). The conductivities of the megaregolith and the underlying fractured zone are approximated by an effective conductivity of 1.0 W mK^{-1} for the outer 10 km using

$$\frac{l_{\text{total}}}{K_{\text{effective}}} = \sum_{i=1}^{N} \frac{l_i}{K_i} \tag{1}$$

where l_i and K_i are the thickness and the thermal conductivity of the ith layer respectively, and N is the total number of layers. The effect of a very low conductivity regolith of a few meters thick-

TABLE 1

Model properties and parameters used in thermal evolution calculations

Radius	1740 km
Density	3340 kg m^{-3}
Specific heat	1200 J kg^{-1} °C^{-1}
Heat of fusion	400 kJ kg^{-1}
U	20 ppb
Th/U	3.7
K/U	2000

ness, with $K = 0.01$ W mK^{-1} (Langseth et al., 1976), is negligible. Other model parameters are listed in Table 1.

During the initial differentiation event, compositional stratification caused by the sinking of dense cumulates leads to a density stratification. It is expected that the inverted density structure of a magma ocean solidifying by fractional crystallization, calculated by Herbert (1980), is a transient condition, as the low viscosity of this region because of its near-solidus temperature and residual melt would quickly produce a stable density stratification. This would not change the distribution of heat-producing elements which remain in the residual liquids and they will still be concentrated upwards. The intrinsically different source regions required to explain the wide range of mare basalt compositions imply that little or no mixing has occurred in these regions (Turcotte and Kellogg, 1986; Papike et al., 1990). This density stratification is expected to prevent convective overturn in the outer layers of the Moon that are considered in this paper, and heat transfer in this region is by conduction. Radiative heat transfer is accounted for by increasing the temperature-dependent thermal conductivity (Fig. 2). The heat conduction equation

$$C\rho\frac{\partial T}{\partial t} = \frac{1}{r^2}\frac{\partial}{\partial r}\left(r^2 K\frac{\partial T}{\partial r}\right) + A \qquad (2)$$

was solved inside a radially symmetric shell 400 km thick by a finite difference method. In eqn. (2), C is specific heat (assumed constant), T is temperature, t is time, r is radial distance from the center of the Moon, K is temperature-dependent thermal conductivity, and A is time-dependent rate of heat-production. At the outer surface of the shell (the surface of the Moon) the temperature is taken to be 0 °C, and at the inner surface of the shell (at a depth of 400 km) the temperature is equal to the solidus temperature at that depth. The inner surface was assumed to be at constant temperature over the entire time interval considered, from 4.4 to 3.0 Ga, as most thermal evolution models, regardless of their choice of parameters, initial conditions, and heat transfer mechanism, show a nearly constant temperature at this depth over this time interval (e.g. Toksöz and Solomon, 1973; Hubbard and Minear, 1975; Solomon and Chaiken, 1976; Toksöz et al., 1978; Arkani-Hamed, 1979; Binder and Lange, 1980; Chacko and DeBremaeker, 1982); thus, the models studied here should apply equally well to both a Moon initially covered by a magma ocean, and an initially totally molten Moon. The latent heat of fusion and percentage of melt are assumed to be distributed linearly between the solidus and liquidus temperatures (Bottinga and Allègre, 1978). This model may underestimate the degree of partial melting as melting may increase rapidly near the solidus and more slowly at higher temperatures (Bickle, 1986).

Lunar selenotherms for the radially symmetric model are shown in Fig. 3. Small amounts of melt are produced, with a maximum of 10% melt from 4.2 to 4.0 Ga. By 3.3 Ga the outer 320 km has completely solidified and below this depth the amount of melting is less than 2%.

The effects of changing the bulk uranium content, the temperature-dependent thermal conductivity model, and the skin depth of the heat source distribution on the Moon's temperature distribution at 3.4 Ga are shown in Fig. 4. The temperature change shown is relative to a model with a bulk uranium content of 20 ppb, a heat source skin depth of 60 km, and the modified Roy et al. (1981) conductivity (Fig. 2). The bulk uranium content was changed from 20 to 15 ppb (closer to chondritic values), to 30 ppb (Arkani-Hamed, 1979), and to 60 ppb (Toksöz and Solomon, 1973). The temperature-dependent conductivity of the modified Roy et al. (1981) model used in this paper was changed to the higher-conductivity model of Schatz and Simmons (1972). The fairly

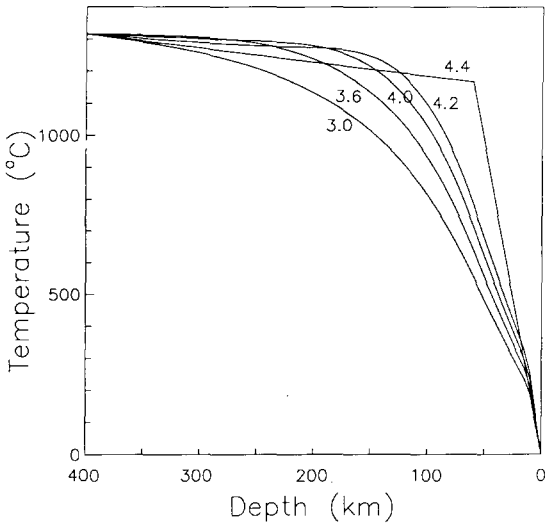

Fig. 3. Lunar selenotherms at five times (4.4, 4.2, 4.0, 3.6, and 3.0 Ga), for the radially symmetric unperturbed model. Selenotherm labelled 4.4 Ga is the initial condition.

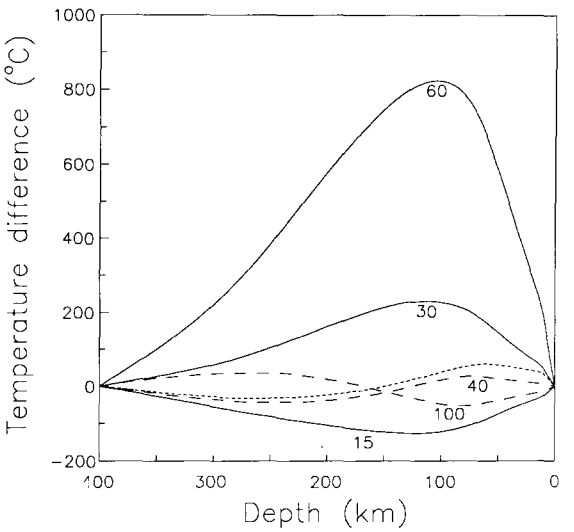

Fig. 4. The effects of the choice of parameters on a selenotherm at 3.4 Ga. Curves labelled 15, 30, and 60 are for bulk uranium contents of 15, 30, and 60 ppb. Curves labelled 40 and 100 are for models with a uranium distribution skin depth of 40 and 100 km. The short-dashed line is for a model with the conductivity model of Schatz and Simmons (1972) (Fig. 2). The change in temperature is relative to a model with a bulk uranium abundance of 20 ppb, a skin depth of 60 km, and modified Roy et al. (1981) conductivity (Fig. 2).

arbitrarily chosen heat source distribution skin depth was changed from 60 to 40 km and to 100 km. Changing the bulk uranium content has the largest effect on temperature, up to 800 °C at a depth of 120 km when it is increased to 60 ppb. Even changes of only 5 ppb can change the temperature by up to 120 °C. Increasing the thermal conductivity, i.e. using the Schatz and Simmons (1972) model, increases the temperature at shallow depths by up to 40 °C and decreases the temperature at greater depths by up to 20 °C. The effect of decreasing the heat source skin depth results in higher temperatures at shallow depths, up to 30 °C higher, whereas increasing the skin depth results in lower temperatures at shallow depths, up to 30 °C lower, and higher temperatures at greater depths, up to 20 °C higher.

The two remelting models studied in this paper result from perturbations of a radially symmetric model with the model parameters listed in Table 1. In the radioactive heating model remelting is due to heating by local enrichment of heat-producing elements, whereas in the thermal insulation model remelting is induced by thermal blanketing caused by a low thermal conductivity ejecta blanket.

2.2. *Radioactive heating model*

It has commonly been assumed in mare basalt petrogenesis models that radioactive heating produced the required remelting (e.g. Hollister, 1975; Brown, 1977; Taylor, 1978; Binder, 1982, 1985). Remelting is assumed to result from local enrichments of heat-producing elements emplaced by the end of the initial differentiation event. These heterogeneities may be related to convection patterns in the magma ocean (Brown, 1977), asymmetrical fractionation of the magma ocean (Warren and Wasson, 1980), locally trapped interstitial late-stage residual liquid (Taylor, 1978), or the late accretion of large planetessimals (Hartmann, 1980; Shervais and Taylor, 1986). Convective motions within the cumulates would very efficiently remove inter-cumulus liquids into overlying regions (Ringwood and Kesson, 1976) and regions of heat-producing element enrichment would be at shallow depths, probably in the latest-stage resid-

ual liquids. Later enrichments might be due to diapirism or the migration of melt from deeper previously undifferentiated regions (Ringwood and Kesson, 1976; Turcotte and Ahern, 1978; Ringwood, 1979) or to the sinking of cumulates and convective overturn because of the gravitational instability of an inverted density structure possibly created by a magma ocean which solidified by fractional crystallization (Herbert, 1980).

Figure 5 shows the geometry used in the radioactive heating models. Many models were run with different sizes and depths of the heat source anomaly. Only two of the models are presented here; in one model the region of enrichment was placed from 60 to 80 km (shallow model), and in the other model from 180 to 200 km (deep model). The heat source anomaly was assumed to be a disk-shaped region with a radius of 75 km ($\theta = 2.5°$) and thickness of 20 km in an otherwise radially symmetric Moon, emplaced by the end of the initial differentiation event at 4.4 Ga. Anomalies of this size can produce excess amounts of melt approximately equal to the volume of basalt in the Imbrium basin.

The effect of radioactive element enrichment was studied quantitatively. The heat conduction equation for axi-symmetric geometry in spherical coordinates,

$$C\rho\frac{\partial T}{\partial t} = \frac{1}{r^2}\frac{\partial}{\partial r}\left(r^2K\frac{\partial T}{\partial r}\right) + \frac{1}{r^2\sin\theta}\frac{\partial}{\partial\theta}\left(K\sin\theta\frac{\partial T}{\partial\theta}\right) + A \qquad (3)$$

was solved by the alternating direction finite difference method (Douglas, 1961). In eqn. (3), θ is the colatitude. At the surface and at a depth of 400 km, the boundary conditions are the same as those of the radially symmetric model. At a colatitude of 50° a zero heat flux boundary condition was imposed, i.e. $\partial T/\partial\theta = 0$ at $\theta = 50°$.

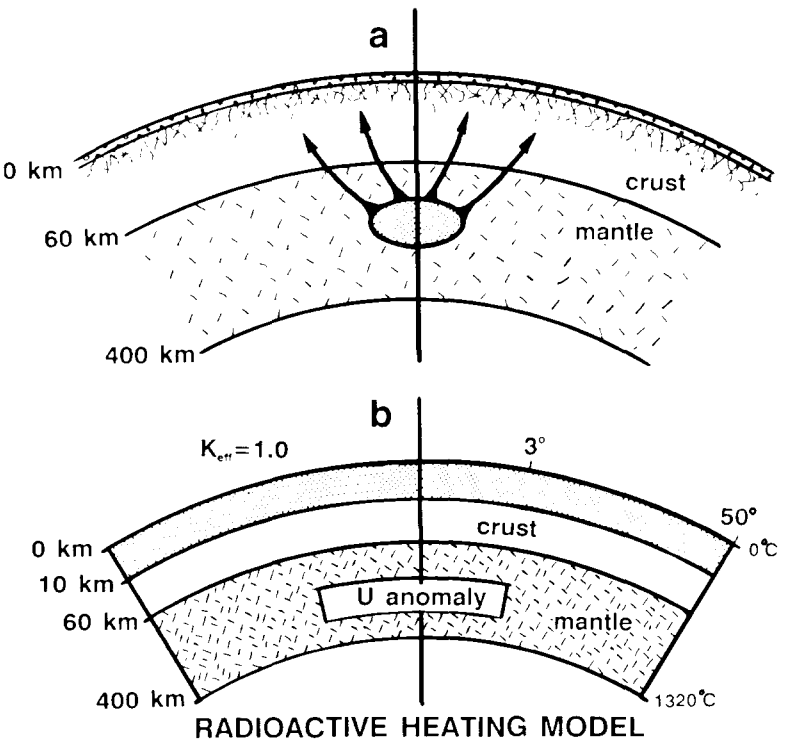

Fig. 5. (a) Radioactive heating model in which partial melting results from regions of enrichment of heat-producing elements. (b) The dimensions, boundary conditions, and properties of the model. The zone of enrichment is a disk-shaped region with a thickness of 20 km and a radius of 75 km.

Figure 6 shows the temperature change along the axis of symmetry as a result of the enrichment of heat-producing elements (called hereafter the anomaly), relative to the radially symmetric Moon. Model temperatures shown are for a shallow anomaly (60–80 km depth) with two and three times enrichment (Figs. 6a and b respectively), and for a deep anomaly (180–200 km depth) with two and five times enrichment (Figs. 6c and d respectively). The same degree of heat-producing element enrichment at shallow and great depths does not have the same effect on temperature because the amount of anomalous heat-producing elements differs owing to the assumed exponential distribution of these elements in the radially symmetric model. The temperature anomaly is created quickly, and its amplitude changes very little over the time interval considered. However, as time progresses, deeper regions warm up for the shallow anomalies, and both deeper and shallower regions warm up for the deep anomalies, relative to the radially symmetric model.

The effect of heat source anomalies on the distribution of melt in the lunar mantle is displayed in Fig. 7. Figs. 7a–d correspond to the models shown in Figs. 6a–d respectively. Each figure consists of seven panels showing a vertical cross-section through the upper mantle and crust at different times for the thermal evolution beginning at 4.2 Ga, and at every 200 m.y. until 3.0 Ga. The dimensions of each panel shown are 1200 km horizontally ($\theta = 20°$) and 400 km vertically. The top of each profile corresponds to the surface of the Moon, and the bottom to a depth of 400 km.

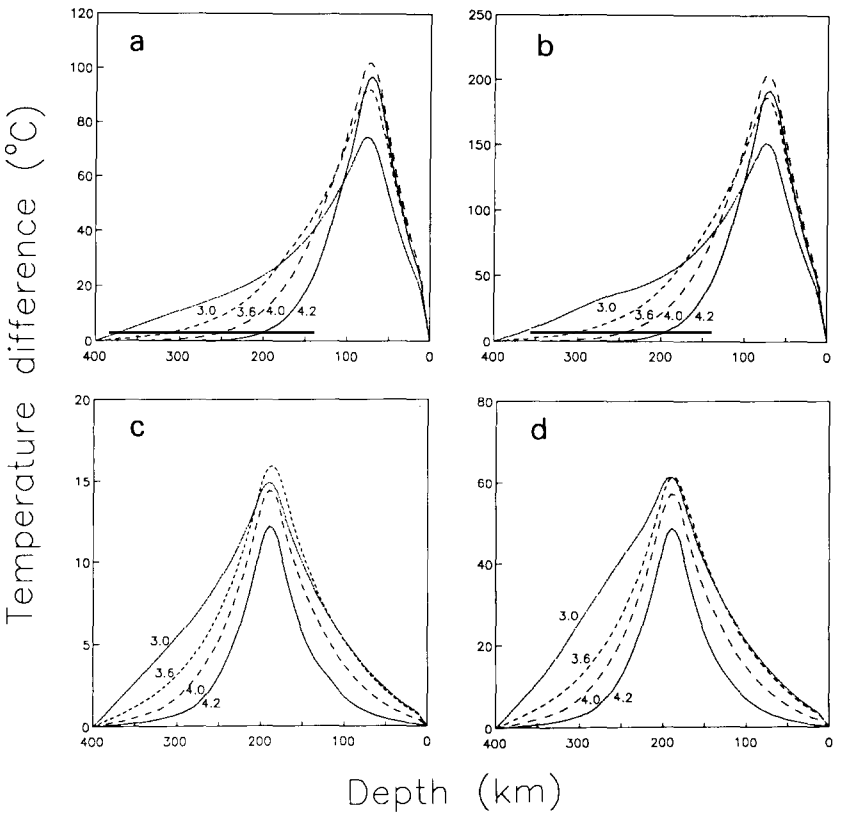

Fig. 6. Temperature differences (°C) between temperatures along a radius passing through the middle of the region of enrichment in the radioactive heating model, and the radially symmetric model. Models shown are for a shallow anomaly with two times enrichment (a) and three times enrichment (b), and a deep anomaly with two times enrichment (c) and five times enrichment (d). The labels on the curves are times in Ga.

The degree of melting has maxima of 14%, 22%, 13%, and 25% in Figs. 7a–d, respectively. Although the degrees of melting are similar for a given degree of enrichment, the change in temperature, as seen in Fig. 6, differs significantly; this is because at greater depths the temperature is closer to the solidus and smaller temperature changes are required for melting, compared with shallow depths, where temperatures are well below the solidus. As the depth of the anomaly increases, smaller and smaller amounts of heat-producing elements are required to produce the same amount of melt. For shallow anomalies, the region of enrichment does not itself melt but instead the region beneath it melts, whereas for deep anomalies the region of enrichment melts. The difference in the depth of the shallowest part of the magma chamber induced by shallow and deep anomalies is only about 20 km even though the difference in the depth of the regions of enrichment is 120 km. The effect of changing the depth of the heat source anomaly within the upper 200 km has little effect on the depth of melting for small degrees of enrichment. For both sets of models, the maximum degree of melting occurs early, at about 4.0 Ga. The degree of melting decreases with time because of the global cooling of the Moon and the decay of the heat-producing elements (by a factor of two over the time interval considered). By 3.0 Ga there is no melt at any depth in all the models. For the models with two times enrichment the degree of melting is less than 5% everywhere by 3.4 Ga and 3.5 Ga for models with a shallow and deep anomaly, respectively. If extraction of melt from the source region requires more than 5% melt (Turcotte and Ahern, 1978; Binder, 1985) radioactive heating models with degrees of enrichment greater than three or four times are required to account for the younger 3.2 b.y.-old basalts.

2.3. *Thermal insulation model*

The important effect of megaregolith insulation on the thermal evolution of asteroids (e.g. Haack

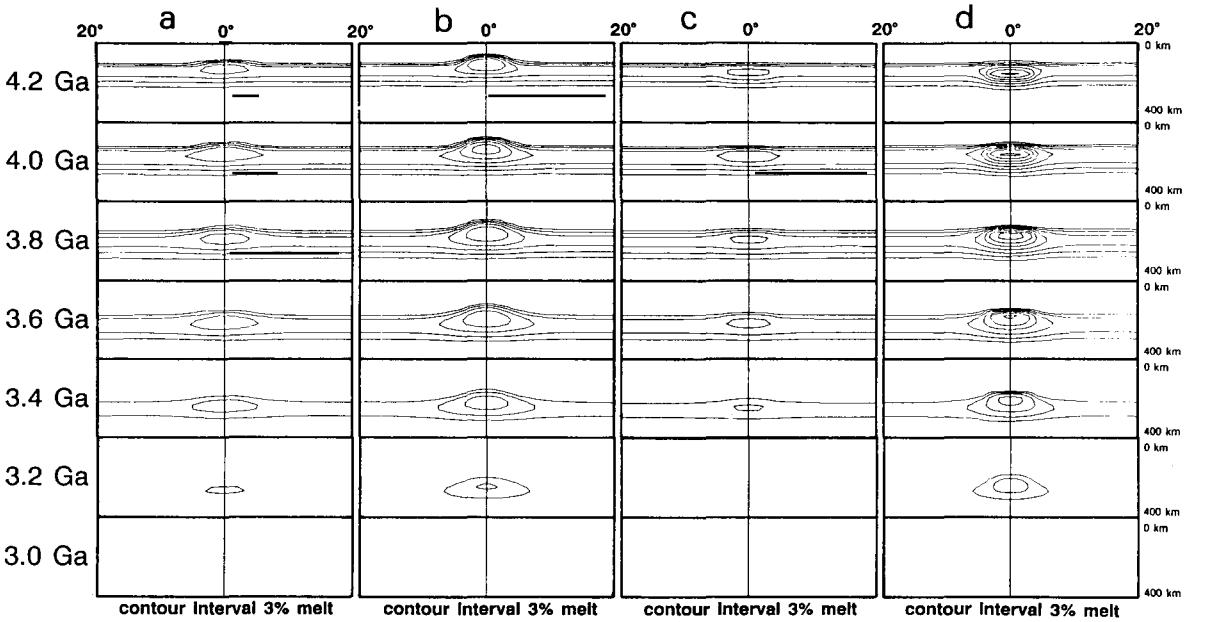

Fig. 7. Distribution of melt for the radioactive heating model. Each figure consists of seven panels at different times in the thermal evolution beginning at 4.2 Ga, and at every 200 m.y. until 3.0 Ga. The horizontal dimension of each panel shown is 1200 km. The top of each panel corresponds to the Moon's surface, and the bottom to a depth of 400 km. The center-line is the axis of symmetry. The figures correspond to models with a shallow anomaly with two times enrichment (a) and three times enrichment (b), and a deep anomaly with two times enrichment (c) and five times enrichment (d). The contour interval is 3% melt.

et al., 1990) and the Moon (Arkani-Hamed, 1973c, 1974; Warren and Rasmussen, 1987) is the basis for the thermal insulation model. Large basin-forming impacts would result in the ejection of large volumes of blocks, loose material, and dust, which would be distributed circumferential to the basin. The high porosity of this material reduces its thermal conductivity, and thus, the impact ejecta blanket acts as a thermal insulator. In the thermal insulation model, impact-created lateral heterogeneities in the thickness of the high-porosity surface layer combined with impact fracturing result in lateral variations of thermal conductivity. The modeling procedure and the radially symmetric Moon in which these perturbations are introduced are identical to those for the radioactive heating model.

Assuming an ejecta blanket of uniform thickness which extends an additional 300 km beyond the edge of a basin with a radius of 300 km, and volumes of ejecta transported beyond an Imbrium-size basin of $(1–8) \times 10^6$ km^3 (McGetchin et al., 1973; Head et al., 1975), ejecta blanket thicknesses range from 1 to 8 km. The thermal conductivity of the ejecta blanket is taken to be the same as that of the homogeneous high-porosity surface layer of 1 km thickness used in the radioactive heating model. Because its thickness is greater, the effective conductivity of the top 10 km beneath and including the ejecta blanket is assumed to range from 0.5 to 0.1 W mK^{-1} i.e. 2–10 times smaller than the effective conductivity of the top 10 km of the radially symmetric model. Because of the large uncertainty in the thermal conductivity and thickness of the ejecta blanket, results were also calculated for models with an ejecta blanket effective conductivity, K_{eff}, of 0.5 W mK^{-1} (one half the conductivity of the radially symmetric model) and 0.1 W mK^{-1} (10 times smaller conductivity than the radially symmetric model). The thickness of the ejecta blanket and megaregolith is limited by sintering (temperature related) and compaction (pressure related). The change of porosity due to sintering is given by (Yomogida and Matsui, 1984)

$$\partial \ln(1-\phi)/\partial t = A\sigma/G^3 \cdot \exp(-Q/RT) \qquad (4)$$

where ϕ is the porosity, σ is the effective stress, G is the grain size (cm), R is the gas constant (kcal K^{-1} mol^{-1}), $A = (2–10) \times 10^{-4}$ is a porosity-dependent constant, and $Q = -85 \pm 29$ kcal mol^{-1} is the apparent activation energy. The values of A and Q were determined experimentally by Schwenn and Goetze (1978) for grain boundary diffusion of olivine crystals for temperatures greater than about 0.7 of the melting temperature. If the extrapolation of these parameters is valid at lower temperatures, sintering on time-scales of 1 b.y. becomes important at temperatures of about 600 °C. To reach this temperature at the base of the ejecta blanket, a conductivity less than 0.2 W mK^{-1} is required for a surface layer of 10 km thickness. The effect of pressure may limit the thickness of the ejecta blanket by reducing its porosity. At pressures from 0.1 to 0.2 kbar, from 2.5 to 5 km depths in the Moon, the tensile strength of rocks is exceeded and fractures may begin to close. Porosity should disappear below about 20 km as the compressive strength of rocks is exceeded. The seismic discontinuity at 20 km (Toksöz et al., 1974) is often interpreted as the depth at which porosity is eliminated. Shock-fractured lunar rocks differ significantly from shock-fractured terrestrial rocks in the range of crack closure pressures, these are up to 2 kbar for lunar rocks, compared with 0.5 kbar for terrestrial rocks (Simmons et al., 1975). If higher estimates of early megaregolith thickness, greater than 5 km (Hörz et al., 1983) and 10 km (Hartmann, 1980; Spudis, 1984) and as high as 30–40 km (Cashore and Woronow, 1985), are correct, then the basin-forming impacts would have little effect on the thickness of the megaregolith as the megaregolith would be reduced everywhere by compaction and sintering to its maximum possible thickness within a few hundred million years.

The geometry, boundary conditions, and near-surface conductivities used in the thermal insulation model are shown in Fig. 8. The basin radius is taken to be 300 km, corresponding to an Imbrium-size basin, and a continuous ejecta deposit with uniform thickness and thermal properties is assumed to extend an additional 300 km beyond the basin (Croft, 1985). The rebound of the basin floor after excavation is assumed to be 40 km

(Taylor, 1982). The rebound of the lithosphere results in the rise of a mantle plug (the region between 40 and 100 km is shifted upwards to between the surface and 60 km) and a corresponding upward displacement of heat-producing elements. All of the impact energy is assumed to go into heating the basin ejecta which cools quickly by radiation before resettling on the surface, although the effect of impact heating of non-ejected target material can be very significant (Bratt et al., 1985). The high thermal conductivity of the basin floor is due to temperature-induced sintering of fractured and porous surface material by basin rebound, impact heating and early basin-filling basalts, and the inclusion of a 5 km post-rebound basin depth in eqn. (1) to calculate its effective conductivity. As radioactive heat transfer is much more efficient than heat conduction, the 5 km deep basin is assumed to have infinite conductivity, and thus, the effect of a non-spherical surface can be incorporated into the effective surface conductivity. Three basin ages, 4.4, 4.2, and 4.0 Ga, are modeled after the end of the initial differentiation event at 4.4 Ga. These ages are greater than the Imbrium event (3.86 Ga) but the two lower ages are more typical of some estimates of basin excavation ages (e.g. Baldwin, 1987a, b). The 4.4 Ga event was modeled to study the effect of early impacts, subsequently covered by more recent impacts. The absolute time of the basin-forming event $\pm$ 100 m.y. is not critical to the relative timing of basaltic volcanism with respect to the time of impact.

The effects of the thermal blanket on the temperature beneath the center of the ejecta blanket (at $\theta = 15°$) relative to the radially symmetric Moon are shown in Figs. 9a, b and c, for an effective conductivity, K_{eff}, of the ejecta blanket of 0.5 W mK^{-1}, 0.25 W mK^{-1}, and 0.1 W mK^{-1}, respectively, and for a basin formed at 4.0 Ga. It

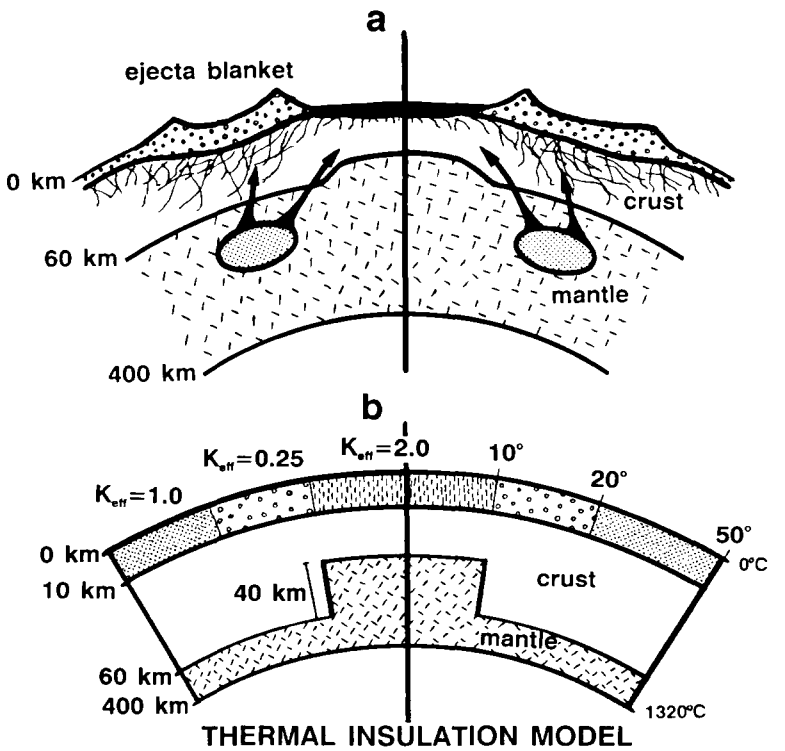

Fig. 8. (a) Thermal insulation model in which partial melting is induced by the blanketing effect of impact ejecta. (b) The dimensions, boundary conditions, and properties of the model. The basin has a radius of 300 km, corresponding to an Imbrium-size basin, and a uniform ejecta blanket extends an additional 300 km beyond the basin.

should be noted that the temperatures for the model with $K_{eff} = 0.1$ W mK^{-1} for the ejecta blanket would lead to sintering at the base of the layer and hence an increase in K_{eff}. The effectiveness of thermal insulation varies almost linearly with the ejecta blanket's conductivity at shallow depths. The insulating effect occurs very quickly near the surface; however, the penetration of the temperature anomaly is slow. For longer times, the boundary condition at 400 km has the effect of reducing and limiting the temperature change. The temperature beneath the center of the basin relative to the radially symmetric Moon is shown in Fig. 9d. Initially, at depths of about 100 km the temperature is higher than for the radially symmetric model because of the rebound of hotter mantle material, but the temperature decreases within 400 m.y. and the temperature is lower than for the radially symmetric model because of the high-conductivity surface layer over the basin and the uplift of heat-producing elements. The warming beneath the basin at depths greater than 200 km after 3.4 Ga is due to the diffusion of heat laterally from beneath the adjacent ejecta blanket.

The distribution of melt for the model with $K_{eff} = 0.25$ W mK^{-1} is shown in Figs. 10a, b and c at seven time intervals of 200 m.y., after an impact at 4.0 Ga, 4.2 Ga, and 4.4 Ga, respectively. Each figure consists of seven panels similar to Fig. 7 for the radioactive heating model; however, the horizontal dimension of each panel is 1800 km ($\theta = 30°$). Perturbations beyond $\theta = 30°$ are negligible. The maximum percentage melt occurs between 3.6 and 3.2 Ga. The maximum degrees of partial melting are 13%, 19%, and 26% for basins formed at 4.0, 4.2, and 4.4 Ga, respectively. Over

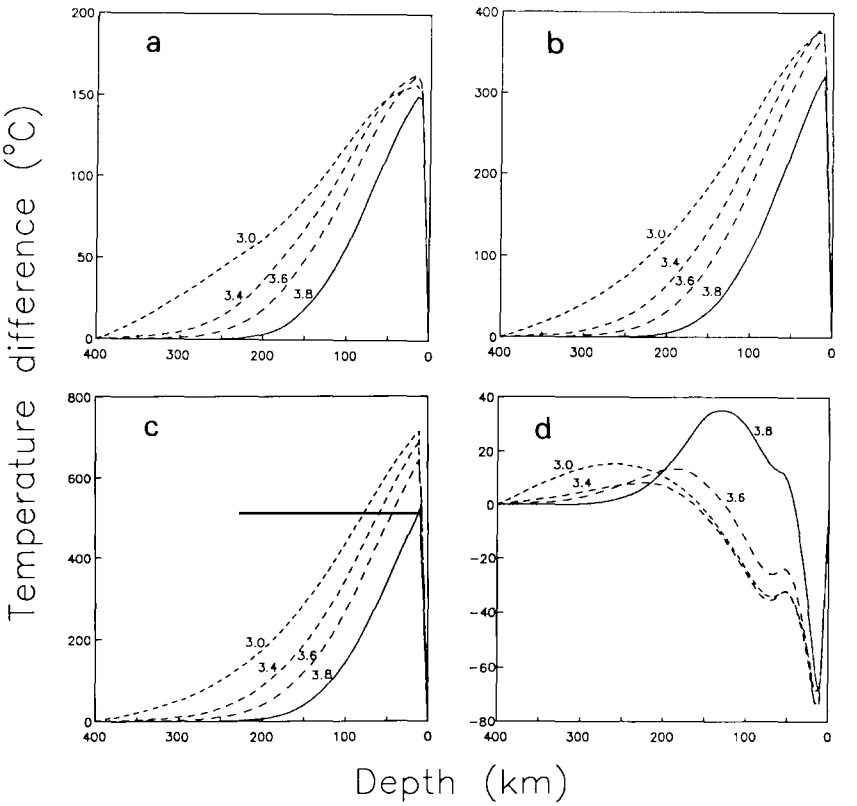

Fig. 9. Temperature difference (°C) along a radius passing through the middle of the thermal ejecta blanket in the thermal insulation model, and the radially symmetric model for conductivities of 0.5 W mK^{-1} (a), 0.25 W mK^{-1} (b), and 0.1 W mK^{-1} (c). The temperature difference beneath the basin is shown in (d). The labels on the curves are the times in Ga.

the first 200 m.y. after impact, for basins formed at 4.2 and 4.0 Ga, the region beneath the basin has the highest degree of melting; this is the result of mantle uplift beneath the basin, whereas the region beneath the ejecta blanket is only beginning to heat up. However, as the impact age increases, the effect of mantle uplift becomes relatively smaller, and for a basin formed at 4.4 Ga the highest degree of melting after 200 m.y. is beneath the ejecta blanket. Qualitatively, the effects of changing the conductivity of the ejecta blanket are identical; however, the degree of melting changes to a maximum of 7%, 13%, and 35% at 3.2 Ga for models with K_{eff} of 0.5 W mK^{-1}, 0.25 W mK^{-1}, and 0.1 W mK^{-1}, respectively (see Figs. 11a and b). The high near-surface temperatures induced by a blanket with a conductivity of 0.1 W mK^{-1} would probably lead to sintering and to a corresponding increase in conductivity. The volumes of excess melt induced by thermal blanketing are, in general, more than one order of magnitude larger than the volume of basalts in an Imbrium-sized basin. The temperature anomalies predicted by the thermal insulation model are consistent with the higher near-surface temperatures surrounding the Serenitatis basin inferred from electrical conductivity measurements, which were previously interpreted as being a result of the removal of heat and heat-producing elements by basalt extrusion (Dyal and Daily, 1979; Vanyan et al., 1979). The effect of basalt removal is much smaller than the thermal insulation effect.

The motivation for developing the thermal insulation model is that it relates the spatial distribution of the maria to the cause of remelting. The heterogeneities responsible for remelting in this model are impact induced, and the remelting is indirectly impact triggered. The thermal insulation model used is similar to those used by Arkani-Hamed (1973c, 1974), but the distribution of heat sources has been revised in accordance with the qualitative model of Taylor and Jakes (1974)—instead of being distributed exponentially to the surface, the maximum abundance occurs at depths from 60 to 80 km. This has the effect of increasing the temperatures beneath the ejecta blanket more than in the earlier models presented by Arkani-Hamed (1973c, 1974). The melting anomalies in

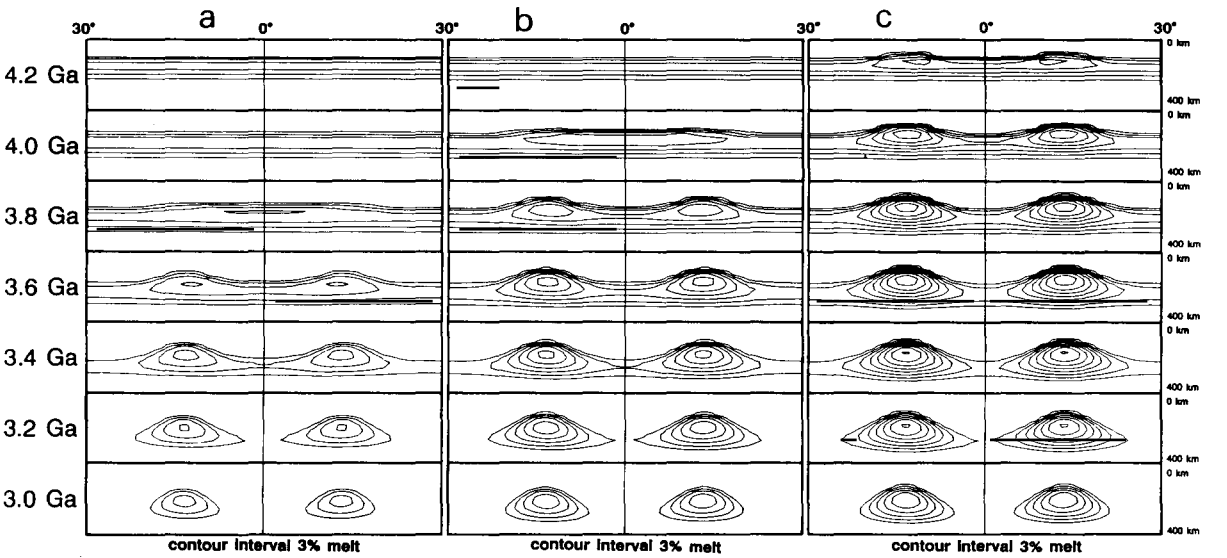

Fig. 10. Distribution of melt for the thermal insulation model. Each figure consists of seven panels at different times in the thermal evolution beginning at 4.2 Ga, and at every 200 m.y. until 3.0 Ga. The horizontal dimension of each panel shown is 1800 km. The top of each panel corresponds to the Moon's surface, and the bottom, to a depth of 400 km. The center line is the axis of symmetry. Ejecta blanket effective conductivity is 0.25 W mK^{-1}. The figures correspond to basin formation ages of 4.0 Ga (a), 4.2 Ga (b), and 4.4 Ga (c). The contour interval is 3% melt.

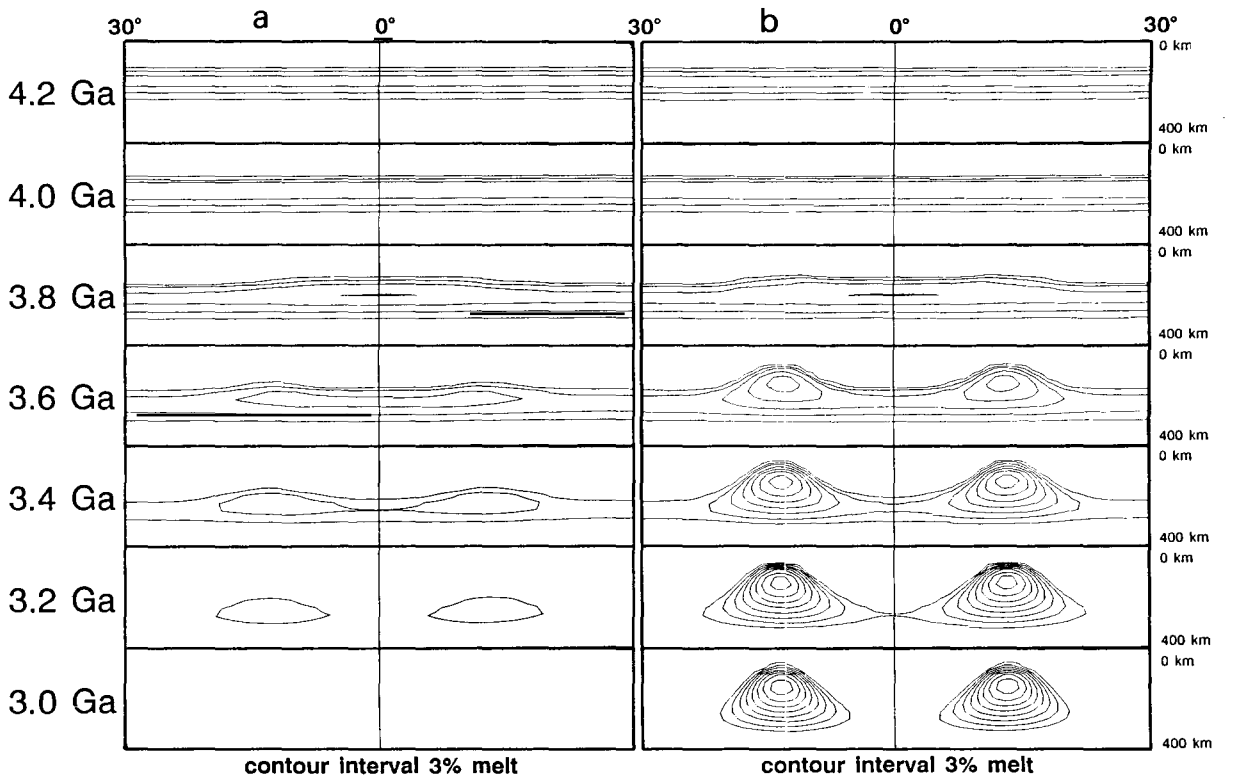

Fig. 11. Distribution of melt at seven times for the thermal insulation model for ejecta blankets with an effective conductivity of 0.5 W mK^{-1} (a) and 0.1 W mK^{-1} (b) (see Fig. 10 for description and explanation). Contour interval is 3% melt.

the earlier models are due to perturbations in the thickness of the solid lithosphere overlying a partially molten interior which thickens about 100 km from 4.0 to 3.0 Ga for a radially symmetric Moon; this is largely a result of the higher bulk uranium content of 60 ppb (Arkani-Hamed, 1973c) and 30 ppb (Arkani-Hamed, 1974). Also, a simulated convection in the partially molten region was used in the earlier models, which enhances the upward heat transfer from the deeper interior and thus reduces the cooling rate of the near-surface regions. In the models presented here, the melting anomalies are magma chambers in a solid lithosphere.

3. Discussion

The plausibilities of both remelting models are evaluated by comparing the consequences of the thermal evolution calculations with observations and measurements. These observations and measurements provide constraints on the models. As only shallow sources are considered here, in effect, the constraints test the feasibility of shallow source regions in a static Moon.

3.1. Chronology

The question of whether there was a time delay between basin formation and basin filling or whether mare volcanism has been a continuous process since basin excavation, is an important time constraint for thermal models. Based on crater counts (Baldwin, 1987b), viscous relaxation models of basins (Baldwin, 1987a), and K–Ar radiometric ages of selected ejecta samples (Schaeffer, 1977) the ages of the basins are calculated to range from 4.3 to 3.83 Ga. However, the absence of impact melts older than 3.9 Ga (Ryder,

1990) and widespread shock metamorphism of the surface at about 3.9 Ga (Wasserberg et al., 1977) suggest that the large nearside basins may have all been formed over a relatively short period of time, lasting about 50–100 m.y. It is now recognized that mare volcanism extended to pre-basin formation times (e.g. Taylor et al., 1983). The extent of pre-basin mare volcanism cannot be determined (Ryder and Taylor, 1976), but its widespread extent, including the far side, is suggested by the distribution of dark-haloed craters (Schultz and Spudis, 1979) and recent spectral images by the Galileo spacecraft (see EOS, 1991, p. 1). Most returned mare basalt ages range from 3.8 to 3.2 b.y. (Geiss et al., 1977), and from crater counting, basin filling is generally thought to have lasted from 3.8 to 2.5 Ga (Boyce, 1976), and possibly to as recently as 1 Ga (Schultz and Spudis, 1983), with most filling occurring from 3.8 to 3.6 Ga (Head, 1976).

The radioactive heating models produce the largest amount of melt early, from about 4.2 to 4.0 Ga, and the volume of melt decreases over time because of the decay of the heat-producing elements and the secular cooling of the Moon. Thus, radioactive anomalies emplaced early in lunar history, by the end of the initial differentiation event, would probably result in extensive pre-basin mare volcanism. The prolonged production of melt would require very large degrees of heat-producing element enrichment; enrichment large enough for more than 50% melt to exist at about 4.2 Ga. Such large amounts of melt early in the Moon's history would probably be extruded and much of the heat-producing elements responsible for the melting, very efficiently reducing the enrichment. Thus, even with substantial initial enrichment, sufficient degrees of partial melting would probably not extend past 3.8 Ga. For enrichment at shallow depths, very little of the enriched zone melts and the extraction of basalts would have less of an effect on subsequent melting than the extraction of melt produced by enrichments at greater depths where the enriched zone itself melts.

The thermal insulation model induces and enhances the degree of partial melting beneath the ejecta blanket. There is a period of time, about 200 m.y., between an impact and the creation of a magma chamber, suggesting a delay between basin excavation and basin-filling. If the ages inferred from most of the returned samples (e.g. Geiss et al., 1977) and crater counts on surface flows and pre-mare craters (e.g. Boyce, 1976) are correct, then there are delays of at least 50–100 m.y. between significant basin filling and basin excavation, even if the basins formed during a terminal cataclysmic event at about 3.9 Ga (e.g. Ryder, 1990). If basin ages are much older (e.g. Baldwin, 1987a, b), and mare ages are representative of major basin filling, then possible delays range from 100 to 500 m.y. The thermal insulation model is consistent with a delay between volcanism and basin formation. However, this delay might not be observed in the ages of basin fill if the melt was induced by pre-existing thermal blankets from earlier impacts. If models which ascribe older ages to the basins are correct, then the earliest flows in the Imbrium basin, for example, might be due to the thermal blanketing effect of older nearby basins such as Serenitatis. This model also maintains a large degree of melting until 3.0 Ga, when calculations were stopped, and might account for the extended duration of volcanism in a cooling Moon.

The earliest stages of volcanism in the thermal insulation model might not be due to the effect of the ejecta blanket, but rather to the initial effect of the uplifted mantle, enhanced by impact heating (an effect not included here). Both uplift and impact heating temperature perturbations essentially disappear before about 500 m.y. after impact (Bratt et al., 1985). After about the first 200 m.y. the effect of the insulating blanket may be more significant. Basin filling may have been characterized by a migration of the source region from beneath the basin as it cools, to beneath the adjacent ejecta blanket as this region warms up. In Mare Orientale, the small volume of flows allows for a good mapping of the temporal history of volcanism: the largest central basalts (volumetrically) are roughly 130 m.y. younger than the basin, and the two smaller regions in the outer rings (over the ejecta blanket), Lacus Autumni and Lacus Veris, are about 400–500 m.y. younger than the basin (Greeley, 1976). The thermal insulation effect would not result in the most volumetrically

significant flows occurring so early, but rather 300–400 m.y. later, and is entirely consistent with the later flows, both in time and in space. The smaller volume of basalts in Orientale compared with Imbrium might be due to the young age of the Orientale basin (3.83 Ga) and smaller size, i.e. cooler Moon, and thinner ejecta blanket (Arkani-Hamed, 1974). Smaller basins should exhibit a greater delay between formation and the beginning of volcanism because of a smaller and thinner ejecta blanket, and younger basins should induce less melting with a longer time delay (see Fig. 10).

As it is unlikely that regions with large degrees of partial melting can persist for a long time without the extraction of melt, the thermal evolution models were recalculated, and melt was removed whenever the degree of partial melting exceeded 5%. Melt migration would probably require more than 5% melt on the Moon (Turcotte and Ahern, 1978), but Binder (1985) suggested that melt will leave the source region when the source reaches 25–30% melt. Lu–Hf, Sm–Nd, Sr–Rb, and total REE data suggest less than 10% melting of a cumulate source (Unruh et al., 1984). Heat-producing elements were assumed to partition entirely into the melt and the removal of melt removes a corresponding proportion of heat-producing elements from the source region to the Moon's surface. For this simplified extrusion model, melt is removed even for the radially symmetric, unperturbed Moon. Allowing for melt extraction, Figs. 12a and b show the distribution of melt for two representative radioactive heating models, one with a shallow heat-source anomaly with three times enrichment, and a second with a deep heat-source anomaly with five times enrichment; melt disappears entirely by 3.7 and 3.75 Ga and extrusion ends by 4.1 and 4.15 Ga, respectively. For the thermal insulation model with an ejecta blanket effective conductivity of 0.25 W mK^{-1} (Fig. 12c), melt disappears by 3.05 Ga and extrusion ends by 3.4 Ga. Even for this simple

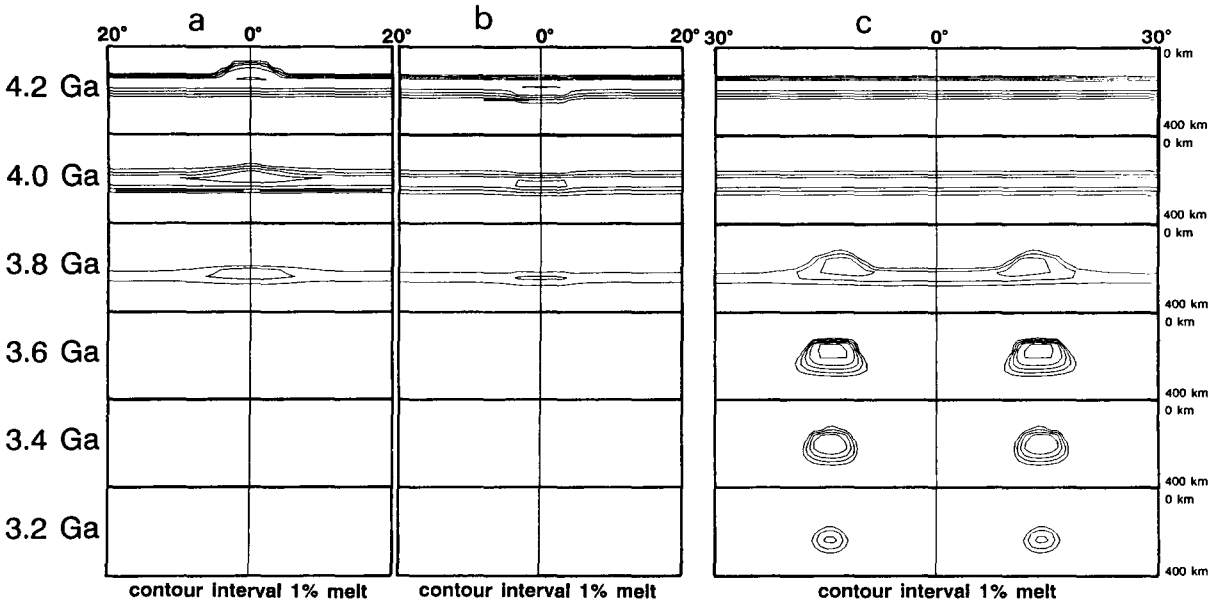

Fig. 12. Distribution of melt for the melt extraction models for the radioactive heating model with a shallow anomaly with three times enrichment (a) and a deep anomaly with five times enrichment (b), and the thermal insulation model with a basin age of 4.0 Ga and an ejecta blanket with an effective conductivity of 0.25 W mK^{-1} (c). Melt is removed to the surface when the degree of melting exceeds 5%. Each figure consists of six panels at different times in the thermal evolution beginning at 4.2 Ga, and at every 200 m.y. until 3.2 Ga. The horizontal dimension of each panel is 1200 km (a, b) and 1800 km (c). The top of each panel corresponds to the Moon's surface, and the bottom to a depth of 400 km. The center-line is the axis of symmetry. The contour interval is 1% melt.

melt removal model, the difference between the two remelting models shown in Fig. 12 is significant; melt extrusion stops more quickly for a deep heat-source anomaly than a shallow anomaly, and only the thermal insulation model allows for the persistence of melt for an extended period of time.

3.2. *Mascon support*

Large positive gravity anomalies are associated with the circular mare basins. The thickness of the mare basalts ranges from a few hundred meters in the irregular maria (Hörz, 1978) to up to 8 or 9 km in the center of the large basins (Solomon and Head, 1979). The absence of positive Bouguer anomalies over the highlands and positive free-air anomalies over unfilled basins (Bills and Ferrari, 1980) imply that the mascons, the mass concentrations responsible for the gravity anomaly, are limited to the filled circular basins. These mascons are the result of rapid isostatic rebound after impact excavation and the subsequent mare filling (Phillips and Lambeck, 1980). The support of these density perturbations for 3.5 b.y. requires a strong upper mantle beneath the mascons; estimated viscosities during the period of basin formation and mare filling are of the order of 10^{25}–10^{26} Pa s^{-1} (Arkani-Hamed, 1973b; Baldwin, 1987a) and of the order of 10^{27}–10^{28} Pa s^{-1} for the last 3 b.y. (Arkani-Hamed, 1973a).

The support of mascons for over 3 b.y. requires a strong upper mantle beneath the mascon. In the radioactive heating models, a mascon emplaced over the region of enrichment might not be very well supported as a result of the temperature related decrease in viscosity. However, if the basalts flowed into low lying areas and basins, and did not accumulate directly above their source, the mascon may be better supported. This would require significant lateral displacement of the basalt for a single source region as the source region must be large enough to account for the volume of basalt. However, many small source regions would not have as large an effect on the viscosity. In addition, removal of melt to form the mascon removes heat and radioactive elements, reducing the temperature anomaly and increasing the viscosity. In the thermal insulation model the region beneath the basin cools more quickly than the region beneath the ejecta blanket and highlands, and the mascon would be best supported by the upper mantle beneath the basin.

The viscosities of both remelting models were studied quantitatively; the viscosities of the models were calculated based on a power creep law for dry websterite (Ave Lallemont, 1978),

$$\eta = \frac{\sigma}{\dot{\epsilon}} = A\sigma^{1-n} \exp(Q/RT) \tag{5}$$

where η is the viscosity, σ is the deviatoric stress, $\dot{\epsilon}$ is the strain rate, R is the gas constant, $A = 10^{-2}$ kbar^n s, $Q = 77.9$ kcal/mol^{-1} is the activation energy, and $n = 4.3$. Dislocation creep dominates for stresses greater than 1 bar whereas diffusion creep dominates for stresses less than 0.1 bar (Turcotte and Schubert, 1982). A change in deviatoric stress from 1 bar to 1 kbar changes the viscosity by 10 orders of magnitude (fig. 3b of Solomon et al., 1982). However, because the deviatoric stresses in the Moon are not known, and because of the uncertainty in extrapolating the high temperature measurements to lower temperatures, the absolute values of viscosity were not calculated. As the temperature dependence of both diffusion and dislocation creep varies linearly with $\exp(Q/RT)$, and assuming that the stresses at a given depth do not change significantly with time, the change in viscosity can be calculated by

$$\ln \eta_2 - \ln \eta_1 = \frac{Q}{R}\left(\frac{1}{T_2} - \frac{1}{T_1}\right) \tag{6}$$

where the subscripts denote values at different times or places. The secular change in viscosity as a function of depth from 4.0 to 3.0 Ga for the radially symmetric model is shown in Fig. 13a. Over the period from 4.0 to 3.0 Ga, the period of mascon formation, the viscosity of the outer 200 km increases by 1–4 orders of magnitude, in agreement with the viscosity increase estimated from mare subsidence during this period (Arkani-Hamed, 1973b). The change in viscosity was also calculated for the radioactive heating models and thermal insulation models. Figure 13b shows the lateral viscosity variations as a result of temperature differences between the radially symmetric

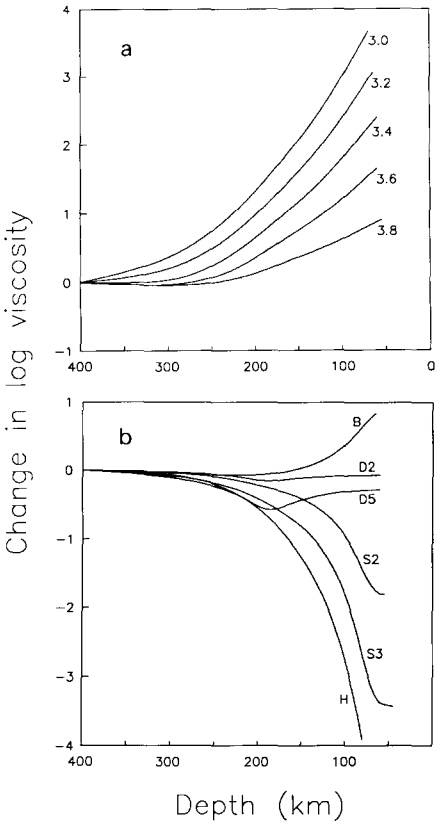

Fig. 13. (a) The change in viscosity with time for the radially symmetric model relative to the viscosity at 4.0 Ga. The numbers on the curves are the times (billions of years ago). (b) Lateral viscosity variations because of temperature differences between the radially symmetric model and the perturbed models at 3.4 Ga. Curves are for the radioactive heating model with a shallow region of heat-source enrichment with two times enrichment and three times enrichment (S2, S3) and a deep region of enrichment with two times enrichment and five times enrichment (D2 and D5), and the thermal insulation model (a basin age of 4.0 Ga and an ejecta blanket effective conductivity of 0.25 W mK^{-1}) beneath the ejecta blanket (H) and beneath the basin (B).

model and the perturbed models at 3.4 Ga. In the radioactive heating models (curves S2, S3, D2, and D5) the temperatures used are along the axis of the anomaly. In the thermal insulation model, the temperatures used are the maximum temperature increases beneath the ejecta blanket (curve H) and along the axis of symmetry of the basin (curve B).

The viscosity change over time is the combination of the radial increase because of the secular cooling of the Moon of Fig. 13a, a significant increase (Baldwin, 1987a), and the lateral variations shown in Fig. 13b. The height and jaggedness of the Orientale and Imbrium rims have probably not changed significantly since their formation (Baldwin, 1987b), implying that the secular increase in viscosity since the formation of older basins may have been comparable with the viscosity decrease beneath the ejecta blanket. The absence of positive free-air gravity anomalies around Serenitatis and Imbrium, and in fact, the presence of negative anomaly rings (Fig. 5, Bills and Ferrari, 1980), implies that the relaxation of basin rim heights, despite their long wavelength, would be determined by the viscosity at shallow depths in the crust. The relaxation of jaggedness, because of its short wavelength, also would involve only shallow depths. Thus, although Fig. 13b suggests that the viscosity decrease beneath the ejecta blanket dominates over the secular increase, rim height relaxation is controlled by near-surface viscosity, which is always very large because of the low near-surface temperatures. If this is the case, the preservation of rim height and jaggedness does not provide a good constraint on lateral viscosity variations, and the decrease in viscosity beneath the ejecta blanket predicted by the thermal insulation model is not inconsistent with the observations. The viscosity decrease shown in Fig. 13b is also the maximum decrease and the viscosity decrease would diminish near the edges of the ejecta blanket. Only the region beneath the basin shows an increase in viscosity, by a factor of about five in the outer 150 km.

In the radioactive heating model, for the degrees of enrichment assumed at great depths from 180 to 200 km (curves D2 and D5) the change in viscosity is very small, whereas the viscosity for a shallow heat-source model (curves S2 and S3) decreases by 1–4 orders of magnitude because of the larger temperature anomaly. Thus, the thermal insulation model is the most likely to be consistent with the mascon support requirement, although the radioactive heating model is acceptable provided that the basalts are deposited at some lateral distance from their source regions, or the source depth is very large.

3.3. *Source region depth*

Over 20 types of mare basalts have been identified; however, they are generally grouped into three categories: high-Al, high-Ti, and low-Ti suites. There is a general trend of decreasing Ti content with age, although the youngest flows in Procellarum and Imbrium are high-Ti basalts. If the melting depth, and hence basalt source region depth, increases with time, a second high-Ti source region underlying the low-Ti source region would be required for the youngest flows. Proposed depths for the sampled high-Ti basalts are of the order of 100–200 km (Hughes et al., 1989), and from 200–400 km (Kesson and Lindsley, 1976) to more than 400 km (Hughes et al., 1988) for the low-Ti suite.

In the cumulate source model (Taylor and Jakes, 1974), a decrease in melting depth over time results in a decrease in Ti content (e.g. Brown, 1977). Radially symmetric models are consistent with a decrease in melting depth, but neither the radioactive heating model nor the thermal insulation model predicts significant change in the depth of the melting anomaly. In the radioactive heating model, different suites might originate from heat-producing element enrichments at different depths; however, there would be no correlation of composition with age, as all suites would erupt early (before basin formation) if these enrichments were emplaced by the end of the initial differentiation at 4.4 Ga. In the thermal insulation model, different source depths might be due to heterogeneities in the thickness and thermal properties of the ejecta blanket. For a thermal blanket with a thermal conductivity of 0.5 W mK^{-1} compared with 0.25 W mK^{-1}, the depth to the top of the magma chamber differs by about 100 km at 3.6 Ga. This difference is at the lower limit of the 100–250 km difference between estimates of source depths for the high-Ti and low-Ti basalts. The possible persistence of melt at shallow depths (about 150 km, a proposed depth for high-Ti basalts) in the thermal insulation model makes it an ideal model for the origin of the late Ti-rich flows in Oceanus Procellarum and Imbrium. These basalts have not been sampled, so no petrologically inferred depth is available for comparison. The constant-temperature boundary condition assumed at a depth of 400 km does not permit a study of the feasibility of the two remelting mechanisms at greater depths. To consider greater depths, the effects of solid-state convection should be included unless the whole Moon was stably density stratified.

3.4. *Extrusion*

The extrusion history of mare basalts has been related to the Moon's global state of stress, such that extrusion occurred during an initial period of expansion, and extrusion ended by a change from global expansion to global contraction (Solomon and Chaiken, 1976; Solomon, 1978), with extrusion being enhanced by local stresses as a result of mascon loading (Solomon and Head, 1979). Tensional stresses act to maintain open conduits and to accentuate stress at the propagating crack tip, whereas compression acts to close conduits, accelerate magma freezing, and impede crack tip propagation (Solomon, 1978).

For a Moon initially covered by a magma ocean, the lithosphere would have been dominated by tensional stresses (Binder and Lange, 1980; Turcotte, 1983) because of the contraction of the outer few hundred kilometers as it cooled around a relatively constant-volume inner mantle. Thus, although the Moon may have been contracting, extensional stresses in the outermost layers, coupled with additional local extensional stresses from regions of melting, would have facilitated magma extrusion for an extended period. However, early impact gardening may have released stresses that had built up before the end of basin formation (Solomon, 1986) thus reducing accumulated tensile stresses over the first 500 m.y. For the magma ocean models studied by Kirk and Stevenson (1989), constrained by a maximum radius change of ± 1 km (Solomon and Chaiken, 1976), the Moon expanded for the first 2 b.y. as a result of the competition between thermal contraction and volume expansion produced by chemical differentiation, resulting in extensional stresses for this period. Also, magma-driven fracturing may be the most important transfer mechanism in the crust and lithosphere (Spence and Turcotte, 1990); if

this is the case, the existence of sufficient melt in the mare basalt source regions may be a sufficient prerequisite for basalt extrusion.

It has commonly been assumed that mare basalts rose hydrostatically, and thus, as the source deepened the basalts rose to higher levels (Solomon, 1975; Wilson and Head, 1981). However, no systematic altitude–age relationship of the lunar maria is observed (Lucchitta and Boyce, 1979), and the eruption of melt may have depended more on the volume of magma produced, and thus on local pressures, than global hydrostatic effects (Muller and Muller, 1980; Whitford-Stark, 1982). The surfaces of many of the maria (notably Serenitatis, Crisium, Smythii, and Van de Graaff) do not at present lie on an equipotential surface, and a best-fit ellipsoidal surface would require a center of mass that is offset 2.7 km east of the present-day center of mass (Sjogren, 1977). Also, the surfaces of Mare Tranquillitatis and Mare Fecunditatis lie 2 km above this best-fit ellipsoidal surface (Sjogren, 1977). This would suggest that significant subsidence of basins has occurred during mare filling and later by viscous relaxation as a result of mascon loading (Arkani-Hamed, 1973a,b). On the basis of such arguments, it would appear that the existence of depressed regions is not sufficient for their filling, and some type of heterogeneity is responsible for their filling.

4. Conclusions

Both models studied, a radioactive heating model and a thermal insulation model, result in remelting at shallow depths. The radioactive heating model, in which enrichments of heat-producing elements are the heat sources for remelting, results in remelting early in lunar history and would result in extensive pre-basin volcanism, if these enrichments were emplaced by the end of the initial differentiation event. The effect of changing the depth of the enrichment within the top 200 km has a minor effect on the depth of melting. However, melting occurs beneath shallow regions of heat-producing element enrichment, and the extrusion of this melt may not affect the concentration of the heat-producing elements. In the case of deep regions of enrichment, the melting occurs in the region of enrichment and the melt produced early would probably be extruded and would carry with it many of the heat-producing elements responsible for melting. Thus, it is unlikely that heat-producing element enrichments emplaced by the end of the initial differentiation event could be responsible for a significant amount of the basin-filling basalts, although they may be a suitable heat source for pre-basin mare basalts.

In the thermal insulation model, remelting is induced about 150–200 km beneath the ejecta blanket by the low thermal conductivity of basin ejecta blankets. The extended duration of melting beneath the ejecta blanket makes it an ideal model for the origin of the younger high-Ti basalts, possibly including the unsampled high-Ti basalts in Oceanus Procellarum and Imbrium which are between 3.0 and 2.5 b.y. old. The thermal insulation model also predicts a delay between the impact and ejecta blanket induced remelting of about 200 m.y. Such a time lag is consistent with some of the older basin ages if most of the basin filling occurred between 3.8 and 3.6 Ga; however, if the basins formed during a terminal cataclysmic event between 3.9 and 3.8 Ga, any delay is likely to be less than 100 m.y. Early basin filling might have been due to the uplift of deeper and hotter material beneath the basin, to impact heating, or to melt induced by older ejecta blankets. After about 200 m.y., the region beneath the basin is colder than the surroundings because of its higher surface conductivity and the uplift of heat-producing elements, and it is better able to support the mascons. The thermal insulation model explains the spatial relation between the maria and basins, as the volcanism, although not directly triggered by impact, is due to impact-related thermal perturbations.

Acknowledgments

This work was supported by Natural Sciences and Engineering Council of Canada (NSERC) grant no. OGP0041245, and an NSERC undergraduate award to M. Manga. The authors appreciate a constructive review by R.B. Baldwin.

References

Arkani-Hamed, J., 1973a. Viscosity of the Moon. I. After mare formation. Moon, 6: 100–111.

Arkani-Hamed, J., 1973b. Viscosity of the Moon. II. During mare formation. Moon, 6: 112–124.

Arkani-Hamed, J., 1973c. On the formation of the lunar mascons. Proc. Lunar Sci. Conf., 4: 2673–2684.

Arkani-Hamed, J., 1974. Effect of a giant impact on thermal evolution of the Moon. Moon, 9: 183–209.

Arkani-Hamed, J., 1979. Non-linear and finite-amplitude thermal convection in a heterogeneous terrestrial planet. Geophys. J. R. Astron. Soc., 56: 63–80.

Ave Lallemont, H.G., 1978. Experimental deformation of diopside and websterite. Tectonophysics, 48: 1–27.

Baldwin, R.B., 1963. Measure of the Moon. University of Chicago Press, Chicago, 488 pp.

Baldwin, R.B., 1987a. On the relative and absolute ages of seven lunar front face basins. I. From viscosity arguments. Icarus, 71: 1–18.

Baldwin, R.B., 1987b. On the relative and absolute ages of seven lunar front face basins. II. From crater counts. Icarus, 71: 19–29.

Bernett, E.C., Wood, H.L., Jaffe, L.D. and Martens, H.E., 1963. Thermal properties of a simulated lunar material in air and in vacuum. AIAA J., 1: 1402–1407.

Bickle, M.J., 1986. Implications of melting for stabilization of the lithosphere and heat loss in the Archean Earth. Earth Planet. Sci. Lett., 80: 314–324.

Bills, B.G. and Ferrari, A.J., 1980. A harmonic analysis of lunar gravity. J. Geophys. Res., 85: 1013–1025.

Binder, A.B., 1982. The mare basalt source region and mare basalt genesis. Proc. Lunar Sci. Conf., 13: 37–53.

Binder, A.B., 1985. The depths of the mare basalt source region. Proc. Lunar Sci. Conf., 15: 396–404.

Binder, A.B. and Gunga, H., 1985. Young thrust-fault scarps in the highlands: Evidence for an initially totally molten Moon. Icarus, 63: 421–441.

Binder, A.B. and Lange, M.A., 1980. On the thermal history, thermal state, and related tectonism of a Moon of fission origin. J. Geophys. Res., 85: 3194–3208.

Binder, A.B. and Oberst, J., 1985. High stress shallow moonquakes: Evidence for an initially totally molten Moon. Earth Planet. Sci. Lett., 74: 149–154.

Bottinga, Y. and Allègre, C.J., 1978. Partial melting under spreading ridges. Philos. Trans. R. Soc. London, Ser. A, 288: 501–525.

Boyce, J.M., 1976. Age of flow units in the lunar nearside maria based on Lunar Orbiter IV photographs. Proc. Lunar Sci. Conf., 8: 3495–3502.

Bratt, S.R., Solomon, S.C. and Head, J.W., 1985. The evolution of impact basins: Cooling, subsidence, and thermal stress. J. Geophys. Res., 90: 12415–12433.

Brown, G.M., 1977. Two-stage generation of lunar mare basalts. Philos. Trans. R. Soc. London, Ser. A, 285: 169–176.

Cashore, J. and Woronow, A., 1985. A new Monte Carlo model of lunar megaregolith development. Proc. Lunar Sci. Conf., 15: 811–815.

Chacko, S. and DeBremaeker, J.Cl., 1982. The evolution of the Moon: A finite element approach. Moon Planets, 27: 467–492.

Conel, J.E. and Morton, J.B., 1975. Interpretation of lunar heat-flow data. Moon, 14: 263–289.

Croft, S.K., 1985. The scaling of complex craters. Proc. Lunar Sci. Conf., 15: 828–842.

Dickinson, T., Taylor, G.J., Keil, K. and Bild, R.W., 1989. Germanium abundances in lunar basalts: Evidence of mantle metasomatism. Proc. Lunar Sci. Conf., 19: 189–198.

Douglas, J., 1961. A survey of numerical methods for parabolic differential equations. Adv. Comput., 2: 1–54.

Dyal, P. and Daily, W.D., 1979. Electrical conductivity anomalies associated with circular lunar maria. Proc. Lunar Sci. Conf., 10: 2291–2297.

Francl, J. and Kingery, W.D., 1954. Thermal conductivity: IX, Experimental investigation of effect of porosity on thermal conductivity. J. Am. Ceram. Soc., 37: 99–107.

Fujii, N. and Osako, M., 1973. Thermal diffusivity of lunar rocks under atmospheric and vacuum conditions. Earth Planet. Sci. Lett., 18: 65–71.

Geiss, J., Eberhardt, P., Grogler, N., Guggisberg, S., Maurer, P. and Stettler, A., 1977. Absolute time scale of lunar mare formation and filling. Philos. Trans. R. Soc. London, Ser. A, 285: 151–158.

Gold, T., 1956. The lunar surface. Mon. Not. R. Astron. Soc., 115: 585–604.

Golombek, M.P. and McGill, G.E., 1983. Grabens, basin tectonics, and the maximum total expansion of the Moon. J. Geophys. Res., 88: 3563–3578.

Greeley, R., 1976. Modes of emplacement of basalt terrains and an analysis of mare volcanism in the Orientale basin. Proc. Lunar Sci. Conf., 7: 2747–2759.

Haack, H., Rasmussen, K.L. and Warren, P.H., 1990. Effects of regolith/megaregolith insulation on the cooling histories of differentiated asteroids. J. Geophys. Res., 95: 5111–5124.

Hartmann, W.K., 1980. Dropping stones in magma oceans: Effects of early lunar cratering. In: J.J. Papike and R.B. Merrill (Editors), Proceedings of the Conference on Lunar Highlands Crust. Pergamon, New York, pp. 81–89.

Head, J.W., 1976. Lunar volcanism in space and time. Rev. Geophys. Space Phys., 14: 265–300.

Head, J.W., Settle, M. and Stein, R.S., 1975. Volume of material ejecta from major lunar basins and implications for the depth of excavation of lunar samples. Proc. Lunar Sci. Conf., 6: 2805–2829.

Herbert, F., 1980. Time-dependent lunar density models. Proc. Lunar Sci. Conf., 11: 2015–2030.

Hollister, L.S., 1975. Evolution of the Moon between 4.6 and 3.3 AE. Proc. Lunar Sci. Conf., 6: 1159–1178.

Horai, K., 1971. Thermal conductivity of rock-forming minerals. J. Geophys. Res., 76: 1278–1308.

Horai, K. and Winkler, J.L., 1976. Thermal diffusivity of four Apollo 17 rock samples. Proc. Lunar Sci. Conf., 7: 3183–3204.

Hörz, F., 1978. How thick are lunar mare basalts? Proc. Lunar Sci. Conf., 9: 3311–3331.

Hörz, F., Ostertag, R. and Rainey, D.A., 1983. Bunte breccia of the Reis: Continuous deposits of large impact craters. Rev. Geophys. 21: 1667–1725.

Hubbard, N.J. and Minear, J.W., 1975. A physical and chemical model of early lunar history. Proc. Lunar Sci. Conf., 6: 1057–1085.

Hughes, S.S., Delano, J.W. and Schmitt, R.A., 1988. Apollo 15 yellow-brown volcanic glass: Chemistry and petrogenetic relations to green volcanic glass and olivine-normative mare basalts. Geochim. Cosmochim. Acta, 52: 2379–2391.

Hughes, S.S., Delano, J.W. and Schmitt, R.A., 1989. Petrogenetic modeling of 74220 high-Ti orange volcanic glasses and the Apollo 11 and 17 high-Ti mare basalts. Proc. Lunar Sci. Conf. 19: 175–188.

Hulme, G., 1974. Generation of magma at lunar impact crater sites. Nature, 252: 556–558.

Kaula, W.M., 1971. Interpretation of the lunar gravitational field. Phys. Earth Planet. Inter., 4: 185–192.

Keihm, S.J. and Langseth, M.G., 1977. Lunar thermal regime to 300 km. Proc. Lunar Sci. Conf., 8: 499–514.

Kesson, S.E. and Lindsley, D.H., 1976. Mare basalt petrogenesis—A review of experimental studies. Rev. Geophys. Space Phys., 14: 361–373.

Kirk, R.L. and Stevenson, D.J., 1989. The competition between thermal contraction and differentiation in the stress history of the Moon. J. Geophys. Res., 94: 12133–12144.

Kunze, A.W.G., 1974. Lunar mascons: Another model and its implications. Moon, 11: 9–17.

Langseth, M.G., Keihm, S.J. and Peters, K., 1976. Revised lunar heat-flow values. Proc. Lunar Sci. Conf., 7: 3143–3171.

Lucchitta, B.K. and Boyce, J.N., 1979. Altitude–age relationships of the lunar maria. Proc. Lunar Sci. Conf., 10: 2957–2966.

McGetchin, T.R., Settle, M. and Head, J.W., 1973. Radial thickness variation in impact crater ejecta: Implications for lunar basin deposits. Earth Planet. Sci. Lett., 20: 226–236.

Millhollen, G.L., Irving, A.J. and Wyllie, P.J., 1974. Melting interval of peridotite with 5.7 percent water to 30 kbar. J. Geol., 82: 575–587.

Mitzutani, H. and Osako, M., 1974. Elastic-wave velocities and thermal diffusivities of Apollo 17 rocks and their geophysical implications. Proc. Lunar Sci. Conf., 5: 2891–2901.

Muller, O.H. and Muller, M.R., 1980. Near surface magma movement. Proc. Lunar Sci. Conf., 11: 1979–1985.

Papike, J.J., Shearer, C.K. and Galbreath, K.C., 1990. Reading the Moon's volcanic record by ion microprobe analysis of Apollo 14 glass beads. Geology, 18: 295–298.

Phillips, R.J. and Lambeck, K., 1980. Gravity fields of the terrestrial planets: Long-wavelength anomalies and tectonics. Rev. Geophys. Space Phys., 18: 27–76.

Ringwood, A.E., 1979. Origin of the Earth and Moon. Springer-Verlag, New York, 295 pp.

Ringwood, A.E. and Essene, E., 1970. Petrogenesis of Apollo 11 basalts, internal constitution and origin of the Moon. Proc. Lunar Sci. Conf., 1: 769–799.

Ringwood, A.E. and Kesson, S.E., 1976. A dynamic model for mare basalt petrogenesis. Proc. Lunar Sci. Conf., 7: 1697–1722.

Roy, R.F., Beck, A.E. and Touloukian, Y.S., 1981. Thermophysical properties of rocks. In: Y.S. Touloukian and C.Y. Ho (Editors), Physical Properties of Rocks and Minerals. McGraw-Hill, New York, pp. 409–488.

Runcorn, S.K., 1977. Early melting of the moon. Proc. Lunar Sci. Conf., 8: 463–469.

Ryder, G., 1990. Lunar samples, lunar accretion and the early bombardment of the moon. EOS, Trans. Am. Geophys. Union, 71: 313–323.

Ryder, G. and Taylor, G.J., 1976. Did mare-type volcanism commence early in lunar history? Proc. Lunar Sci. Conf., 7: 1741–1755.

Schaeffer, O.A., 1977. Lunar chronology as determined from the radiometric ages of returned lunar samples. Philos. Trans. R. Soc. London, Ser. A, 285: 137–143.

Schatz, J.F. and Simmons, G., 1972. Thermal conductjvity of Earth materials at high temperatures. J. Geophys. Res., 77: 6966–6983.

Schubert, G., Stevenson, D.J. and Cassen, P., 1980. Whole planet cooling and the radiogenic heat-source contents of the earth and Moon. J. Geophys. Res., 85: 2531–2538.

Schultz, P.H. and Spudis, P.D., 1979. Evidence for ancient mare volcanism. Proc. Lunar Sci. Conf., 10: 2899–2918.

Schultz, P.H. and Spudis, P.D., 1983. Beginning and end of lunar mare volcanism. Nature, 302: 233–236.

Schwenn, M.B. and Goetze, C., 1978. Creep of olivine during hot-pressing. Tectonophysics, 48: 41–60.

Shervais, J.W. and Taylor, L.A., 1986. Petrologic constraints on the origin of the Moon. In: W.K. Hartmann, R.J. Phillips and G.J. Taylor (Editors), Origin of the Moon. Lunar Planetary Institute, Houston, TX, pp. 173–201.

Simmons, G., Siegfried, R. and Richter, D., 1975. Characteristics of microcracks in lunar samples. Proc. Lunar Sci. Conf., 6: 3227–3254.

Sjogren, W.L., 1977. Lunar gravity determinations and their implications. Philos. Trans. R. Soc. London, Ser. A, 285: 219–226.

Solomon, S.C., 1975. Mare volcanism and lunar crustal structure. Proc. Lunar Sci. Conf., 6: 1021–1042.

Solomon, S.C., 1978. On volcanism and thermal tectonics on one-plate planets. Geophys. Res. Lett., 5: 461–464.

Solomon, S.C., 1986. On the early thermal state of the Moon. In: W.K. Hartmann, R.J. Phillips and G.J. Taylor (Editors), Origin of the Moon. Lunar Planetary Institute, Houston, TX, pp. 435–452.

Solomon, S.C. and Chaiken, J., 1976. Thermal expansion and thermal stress in the Moon and terrestrial planets: Clues to early thermal history. Proc. Lunar Sci. Conf., 7: 3229–3243.

Solomon, S.C. and Head, J.W., 1979. Vertical movement in mare basins: Relation to mare emplacement, basin tectonics, and lunar thermal history. J. Geophys. Res., 84: 1667–1682.

Solomon, S.C., Comer, R.P. and Head, J.W., 1982. The evolution of impact basins: Viscous relaxation of topographic relief. J. Geophys. Res., 87: 3975–3992.

Spence, D.A. and Turcotte, D.L., 1990. Buoyancy-driven magma fracture: A mechanism for ascent through the lithosphere and the emplacement of diamonds. J. Geophys. Res., 95: 5133–5140.

Spudis, P.D., 1984. Apollo 16 site geology and impact melts: Implications for the geologic history of the lunar highlands. Proc. Lunar Sci. Conf., 15: 95–107.

Stevenson, D.J., 1987. Origin of the Moon—the collision hypothesis. Ann. Rev. Earth Planet. Sci., 15: 271–315.

Taylor, A.T., Shervais, J.W., Hunter, R.H., Shih, C.Y., Bansal, C.L., Wooden, J., Nyquist, N.E. and Laul, L.C., 1983. Pre-4.2 AE mare-basalt volcanism in the lunar highlands. Earth Planet. Sci. Lett., 66: 33–47.

Taylor, S.R., 1978. Geochemical constraints on melting and differentiation of the Moon. Proc. Lunar Sci. Conf., 9: 15–23.

Taylor, S.R., 1982. Planetary Science: A Lunar Perspective. Lunar and Planetary Institute, Houston, TX, 512 pp.

Taylor, S.R. and Jakes, P., 1974. The geochemical evolution of the Moon. Proc. Lunar Sci. Conf., 5: 1287–1305.

Toksöz, M.N. and Solomon, S.C., 1973. Thermal history of the Moon. Moon, 7: 251–278.

Toksöz, M.N., Press, F., Dainty, A.M. and Anderson, K.R., 1974. Lunar velocity structure and compositional and thermal inferences. Moon, 9: 31–42.

Toksöz, M.N., Hsui, A.T. and Johnston, D.H., 1978. Thermal evolutions of the terrestrial planets. Moon Planets, 18: 281–320.

Turcotte, D.L., 1983. Thermal stresses in planetary elastic lithospheres. Proc. Lunar Sci. Conf., 13: 585–587.

Turcotte, D.L. and Ahern, J.L., 1978. Magma production and migration within the Moon. Proc. Lunar Sci. Conf., 9: 307–318.

Turcotte, D.L. and Kellogg, L.H., 1986. Implications of isotope data for the origin of the Moon. In: W.K. Hartmann, R.J. Phillips and G.J. Taylor (Editors), Origin of the Moon. Lunar Planetary Institute, Houston, TX, pp. 311–329.

Turcotte, D.L. and Schubert, G., 1982. Geodynamics: Applications of Continuum Physics to Geological Problems. Wiley, New York, 445 pp.

Unruh, D. M., Stille, P., Patchett, P.J. and Tatsumoto, M., 1984. Lu–Hf and Sm–Nd evolution in lunar mare basalts. Proc. Lunar Sci. Conf., 14: 459–477.

Urey, H.C., 1952. The Planets: Their Origin and Development. Yale University Press, New Haven, CT, 242 pp.

Vanyan, L.L., Vnuchkova, T.A., Egorov, I.V., Basilevsky, A.T., Eroshenko, E.G., Fainberg, E.B., Dyal, P. and Daily, W.D., 1979. Electrical conductivity anomaly beneath Mare Serenitatis detected by Lunokhod 2 and Apollo 16 magnetometers. Moon Planets, 21: 185–192.

Walsh, J.B. and Decker, E.R., 1966. Effect of pressure and saturating fluid on the thermal conductivity of compact rock. J. Geophys. Res., 71: 3053–3061.

Warren, N. and Trice, R., 1977. Structure in the upper lunar crust. Philos. Trans. R. Soc. London, Ser. A, 285: 469–473.

Warren, P.H. and Rasmussen, K.L., 1987. Megaregolith insulation, internal temperatures and bulk uranium content of the Moon. J. Geophys. Res., 92: 3453–3465.

Warren, P.H. and Wasson, J.T., 1980. Early lunar petrogenesis, oceanic and extraoceanic. In: J.J. Papike and R.B. Merrill (Editors), Proceedings of the Conference on the Lunar Highlands Crust. Pergamon, New York, pp. 155–171.

Wasserburg, G.J., Papanastassiou, D.A., Tera, F. and Huneke, J.C., 1977. Outline of a lunar chronology. Philos. Trans. R. Soc. London, Ser. A, 285: 7–22.

Whitford-Stark, J. L., 1982. Preliminary analysis of lunar extra-mare basalts: Distribution, compositions, ages, volumes, and eruption styles. Moon Planets, 26: 323–338.

Wilson, L. and Head, J.W., 1981. Ascent and eruption of basaltic magma on the Earth and Moon. J. Geophys. Res., 86: 2971–3001.

Wones, D.R. and Shaw, H.R., 1975. Tidal dissipation: A possible heat source for mare basalt magmas (abstr.). Lunar Sci., VI: 878–880.

Yomogida, K. and Matsui, T., 1984. Multiple parent bodies of ordinary chondrites. Earth Planet. Sci. Lett., 68: 34–42.